

# Importance of Receptor Flexibility in Binding of Cyclam Compounds to the Chemokine Receptor CXCR4

Alfonso R. Lam, Supriyo Bhattacharya, Kevin Patel, Spencer E. Hall, Allen Mao, and Nagarajan Vaidehi\*

Division of Immunology, Beckman Research Institute of the City of Hope, Duarte, California 91010, United States

Received August 6, 2010

We have elucidated the binding sites of four moncyclam and one bicyclam antagonist AMD3100, in the human chemokine receptor CXCR4. Using the predicted structural models of CXCR4, we have further predicted the binding sites of these cyclam compounds. We used the computational method LITiCon to map the differences in receptor structure stabilized by the mono and bicyclam compounds. Accounting for the receptor flexibility lead to a single binding mode for the cyclam compounds, that has not been possible previously using a single receptor structural model and fixed receptor docking algorithms. There are several notable differences in the receptor conformations stabilized by moncyclam antagonist compared to a bicyclam antagonist. The loading of the Cu<sup>2+</sup> ions in the cyclam compounds, shrinks the size of the cyclam rings and the residue D262<sup>6,58</sup> plays an important role in bonding to the copper ion in the moncyclam compounds while residue E288<sup>7,39</sup> is important for the bicyclam compound.

## INTRODUCTION

Chemokines and their receptors play a fundamental role in carrying diverse messages which are critical in mediating both innate and adaptive immunity.<sup>1</sup> Chemokines function by binding to chemokine receptors that belong to the superfamily of membrane proteins known as the G-protein coupled receptors (GPCRs),<sup>2</sup> that are clinically important drug targets.<sup>3</sup> In human, there are 19 different types of chemokine receptors that respond to over forty different chemokines known today.<sup>4–6</sup> The chemokine receptor CXCR4 and its chemokine stromal-derived-factor-1 (SDF-1) play an important role in many human cancers, homing of hematopoietic stem cells in the bone marrow,<sup>7</sup> as well as mediating HIV entry into the cell.

There has been a considerable amount of effort put into the development of CXCR4 antagonist over the years,<sup>8</sup> given their pathological role in cancers. Small molecule inhibitor such as AMD3100 is in clinical use now for homing of stem cells and is a potent and high affinity bicyclam compound that is highly specific for CXCR4. It inhibits the HIV cell entry and the binding and function of CXCL12.<sup>9</sup> AMD3465, a moncyclam derivative, retains all the biological properties of AMD3100 (inhibition of HIV cell entry and blockage of CXCL12) with an improved effectiveness as a CXCR4 antagonist.<sup>10–12</sup> These mono- and bicyclam compounds are also promoters of chemotaxis and hence lead to homing of stem cells in the bone marrow.<sup>13–16</sup> The development of noncyclam compounds such as AMD11070 helped not only to reduce the molecular size and formal charge on the HIV-1 inhibitors, but also to gain oral bioavailability.<sup>17</sup>

The binding site of the cyclam compounds and their derivatives in CXCR4, has been studied using site directed mutagenesis, and their effects on inhibition of HIV entry.<sup>18–22</sup>

Gerlach et al.<sup>23,24</sup> first postulated that the potent inhibitor AMD3100 should bind to the CXCR4 receptor through D171<sup>4,60</sup> and D262<sup>6,58</sup> residues. Here, we have used the Ballesteros and Weinstein numbering<sup>25</sup> for class A GPCRs. [In the Ballesteros and Weinstein numbering system for class A GPCRs, the first number denotes the transmembrane (TM) helix in which the residue is located, and the second number denotes the position of the residue with respect to the most conserved residue in that helix across class A GPCRs.] Further studies made by Hatse et al.<sup>26</sup> confirmed the relevance of these residues in binding. Recently, Rosenkilde et al.<sup>20,21</sup> performed extensive point mutation study on the residues located on the extracellular half of the transmembrane helices and in the extracellular loop 2 (ECL2) to identify additional residues involved in binding of the bicyclam compound AMD3100 and other moncyclam derivatives such as AMD3465, AMD3389, and AMD3529 shown in Figure 1. This study clearly elucidated the differential effects of mutations of residues D171<sup>4,60</sup>, Q200<sup>5,39</sup>, D262<sup>6,58</sup>, H281<sup>7,32</sup>, and E288<sup>7,39</sup> on binding of AMD3100 and its derivatives shown in Figure 1. They showed that residue mutations D171N, D262N, and E288A significantly affect the binding of AMD3100 to CXCR4, and have differential effects on other cyclam ligands. Other residue mutations such as Q200W had similar effect as D171<sup>4,60</sup>, while H281A had a significant effect on AMD3465 binding, and not on AMD3100 bicyclam binding. Other residues that affect the binding of AMD3465, but not AMD3100 are H113<sup>3,29</sup>, V196<sup>5,35</sup>, I259<sup>6,55</sup>, I284<sup>7,35</sup>, and T287<sup>7,38</sup>. Wong et al.<sup>22</sup> modeled the binding site of the mono and bicyclam AMD derivatives and concluded that multiple binding sites have to be invoked for binding of mono and bicyclam compounds to account for all the mutagenesis data. To date we do not have a structural model of the binding sites of the cyclam compounds that accounts for all the mutation data in the CXCR4 receptor. In this paper, we have

\* To whom correspondence should be addressed. E-mail: nvaidehi@coh.org.

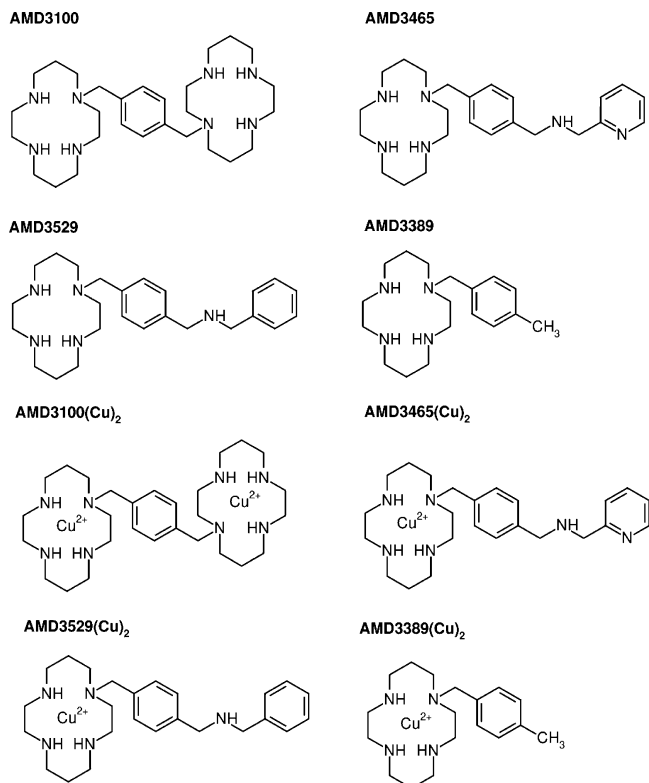


**Figure 1.** Mono- and bicyclam compounds used in this study with their respective copper(II) derivatives.

used an ab initio structure prediction method, and shown that modeling an ensemble of receptor conformations for human CXCR4 describes the dynamics in the receptor structures, known for GPCRs. We have further used a receptor flexible docking protocol and predicted the binding sites of the bicyclam compound AMD3100, and the monocyclam derivatives. We find that receptor conformation stabilized by mono and bicyclam compounds are slightly different. Since the receptor conformational flexibility was accounted for in docking each ligand, we could identify a unified single binding model that explains all the available mutation data for these cyclam compounds. We have also studied the effect of Cu<sup>2+</sup> loaded cyclam compounds on the binding site of these compounds in CXCR4.

#### COMPUTATIONAL METHODS

##### Prediction of Structural Models for Human CXCR4.

We used MembStruk4.30 version<sup>27,28</sup> to predict the ensemble of structural models for the wild-type of human CXCR4. Here we present only the details of the methods as relevant to CXCR4. The TM regions and the hydrophobic maximum were predicted using multiple sequence alignments of all human, rat, and mouse CXC and CC chemokine receptors that showed sequence identity down to 20% and using Tm2ndS method detailed in Trabanino et al.<sup>27</sup> The Tm2ndS uses a multiple sequence alignment and predicts the TM region based on the seven maxima in hydrophobicity over the entire sequence alignment. The predicted TM regions of the receptor are given in Scheme 1.

The next step was to optimize the rotation, translation, and the helical kinks starting from an assembled bundle of the canonical helices built from the TM predictions. Canonical right-handed  $\alpha$ -helices were built for each helix and their

**Scheme 1.** Predicted Transmembrane Regions of CXCR4<sup>A</sup>

NT	1	MEGISIYTSNDYNTTEEMGSDYDSMKEPCFREENANF	36 (36)
TM 1	37	NKIFLPTIYIISIIFTGTIVGNGLVILVMG	64 (28)
LP 1	65	YQKKLRSMTD	74 (10)
TM 2	75	KYRLHLSVAALLFVITLPFWAVDA	98(24)
LP 2	99	VANWYFG	105 (7)
TM 3	106	NFLCKAVHVITYTVNLYSSVLAFISLDRYL	136 (31)
LP 3	137	AI VHATNSQRPRKLLA	152(16)
TM 4	153	EKV VYVGWIPALLLTIPDFIFANVSE	179(27)
LP 4	180	ADD RYICDRFYPNDLWVVV	198(19)
TM 5	199	FQFQHIMVG LPG I VILSCYCIISK	225(27)
LP 5	226	LHSKGHQKR KAL	238(13)
TM 6	239	KTTVILAFFACWL PYI GISIDS FIL	266(28)
LP 6	267	LEI IKQGCE FENTVHKW	283(17)
TM 7	284	I SITE ALAFFHCCLNPIL Y AFLG	306(23)
CT	307	AKFKTSAQHALTS VSRGSSLKILSKGKRG GHSSVSTE ESSSFHSS	352 (46)

<sup>A</sup> The residue numbers are given on the left and right hand sides of the sequence. The total number of residues in each structural segment is given in parentheses.

helical axes were oriented in space according to the helical axes orientations observed in the crystal structure of  $\beta$ 2-adrenergic receptor.<sup>29</sup> The relative translational orientation of the seven helices were optimized by aligning the hydrophobic maximum determined for each helix, to a plane. The rotational orientation was optimized using a combination of hydrophobic moments and molecular dynamics techniques. Thus using the MembStruk4.0 procedure we derived an ensemble of low energy TM barrel conformations for CXCR4. The receptor conformations were chosen by maximum number of interhelical hydrogen bonds (HBs), and the lowest total energy of the protein conformation in explicit lipid bilayer. There are three possible low energy conformations chosen for CXCR4 showing different orientations of TM3, TM5 and TM7. TM5 showed three different low energy conformations, two of which are different orientations of the residue Y219<sup>5,58</sup>. These two orientations correspond to the two orientations of Y223<sup>5,58</sup> in the crystal structure of rhodopsin and opsin.<sup>30–32</sup> TM7 showed two orientations, where the position of E288<sup>7,39</sup> are different. Combinations of these rotational orientations were made and sorted by maximum number of interhelical HBs and total energy. Three best structures were chosen and extra- and intracellular loops were added using Modeler.<sup>33</sup>

**Ligand Docking Methods.** The ligands shown in Figure 1 were built using the Maestro builder from Schrödinger Inc. Minimization of the ligand energy was performed to optimize the geometry with OPLS 2005 force field,<sup>34</sup> with no solvent and a dielectric constant of 1.0. We used PRCG method with 500 iterations and a convergence threshold of 0.05 (Converge on gradient). The Monte Carlo method in the Macromodel module was used to generate multiple conformations for each of the ligand. We used Epik to generate all possible protonated states. The ligand conformations thus generated were clustered with a rmsd distance cutoff of 0.75 Å and the best energy conformation in each cluster was used for docking. The ligands were docked using Glide XP (Schrödinger, Inc.); with scaled van der Waals radii by 0.5. We retained 10 docked poses per ligand. The docked conformations were clustered using xcluster (Schrödinger Inc.) with a distance cutoff of 1.5 Å. The side chain conformations of

the residues within 5 Å of the ligand docked conformation were optimized using Prime module. The binding energies (BE) of the docked poses were calculated as  $BE = PE(\text{ligand in fixed protein}) - PE(\text{ligand in solvation})$ , where BE is the binding energy,  $PE(\text{ligand in fixed protein})$  is the potential energy of the ligand calculated with the protein atoms fixed, and  $PE(\text{ligand in solvation})$  is the potential energy of the ligand calculated with the surface-generalized Born continuum solvation method.<sup>35</sup> The best scoring docked conformations were then visually inspected, and the conformation with the best set of contacts that agree with the mutation data was selected to be refined with LITiCon.

**Computing Receptor Flexibility upon Ligand Binding Using LITiCON Method.** LITiCon is a computational method to map possible perturbations in the helical rotational conformations induced by ligand binding in the TM region of GPCRs. It involves systematic spanning of the receptor conformations involving the helical rotations as a response to the ligand binding. The LITiCon method has been described in detail in previous publications.<sup>36–38</sup> Here, we describe the procedure as it was used for the best docked pose of every ligand in CXCR4: (1) Starting from the ligand docked structure of CXCR4, the first step of LITiCon is to perform simultaneous rotations of all the seven TM helices. Thus, we performed simultaneous rotations of all the seven TM helices within the range  $\pm 10^\circ$ , in  $10^\circ$  increment relative to the initial state. For TM2, we put more emphasis since residue W94<sup>2,60</sup> is far away from the binding site, and it was reported as critical in binding. Thus, we explored a wider range of rotation angles, namely  $\pm 60^\circ$  in  $5^\circ$  increment. (2) Several conformations that were generated by simultaneous rotations of all the seven helices were then optimized as follows:

- For each conformation the side-chain conformations were optimized using SCWRL 3.0. Conjugate gradient minimization of the potential energy of the ligand in the field of the rest of protein was performed until convergence of 0.3 kcal/mol Å rms deviation in force per atom is achieved.
- We then calculated the ligand binding energy as the difference in the potential energy of the ligand with protein fixed, and the potential energy of the free ligand calculated in water using generalized Born solvation method.
- The number of interhelical and ligand–receptor HBs were calculated using HBPLUS 3.0.<sup>39</sup>
- This generates a multidimensional binding energy landscape for each ligand. The local minima were identified, clustered and sorted by total number of interhelical HB and ligand–receptor HB and then by binding energy. The final ligand stabilized receptor structural models were selected based on low binding energy and high number of HBs.

The LITiCon method can be used to analyze the receptor flexibility that is specific to ligand binding. Earlier modeling studies on CXCR4 using rigid receptor models led to the proposal of multiple binding modes for the cyclam compounds. Here, we demonstrate that application of the LITiCon method to include the receptor flexibility leads to a unified single binding mode that satisfies all point mutation studies on binding of cyclam compounds.

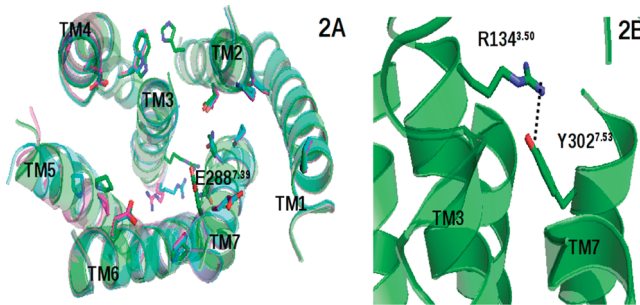


**Figure 2.** (A) Three low-energy receptor conformations chosen from MembStruk predictions. Several differences have been observed in the side chains and main chain of residues in each chosen conformations. For example see E288<sup>7,39</sup>. (B) CXCR4 sequence does not have an acidic residue on TM6 as in other class A GPCRs and therefore no “ionic lock” formed with R134<sup>3,50</sup> residue. One of our three possible conformations for TM3, R134<sup>3,50</sup> residue is making a cation pi interaction with Y302<sup>7,53</sup> as shown.

## RESULTS AND DISCUSSION

**Structural Ensemble of the Wild-Type CXCR4.** The three low-energy receptor conformations chosen from MembStruk predictions are shown in Figure 2. These three conformations differ in the rotation angles of TM3, TM5, and TM7. TM7 shows two possible conformations, one in which the most conserved E288<sup>7,39</sup> residue in TM7 among chemokine receptors, is facing toward TM1, and the other conformation in which it is facing TM3. The conformation in which the residue E288<sup>7,39</sup> is facing TM1, the N298<sup>7,49</sup> of the NPXXY motif, makes a direct HB with D84<sup>2,50</sup>, which in turn makes a HB with N56<sup>1,50</sup>. In the other conformation the HB between N298<sup>7,49</sup> and D84<sup>2,50</sup> is weakened and could become water mediated. All the TM helices in CXCR4 show a kink around the proline residue. This kink is less predominant in TM1 since the proline is at the extracellular edge of TM1. The kink in TM2 in the  $\beta$  adrenergic receptor crystal structures (PDB ID 2RH1 and 2VT4)<sup>40,41</sup> caused by a proline places the extracellular part of TM2 facing TM7 in these structures. The kink on TM2 in rhodopsin (PDB ID 1GZM),<sup>42</sup> is caused by two consecutive glycine residues and this makes TM2 face TM1 in rhodopsin. In chemokine receptors that we have modeled so far CCR1, CCR2, and CCR5,<sup>43,44</sup> using the ab initio structure prediction method (MembStruk), the kink on TM2 places the TM2 facing TM3. This is true in the CXCR4 structure predicted here. Other studies on chemokine receptor modeling have reported similar kinks.<sup>45</sup> Another notable feature about the CXCR4 structural model is that the W161<sup>4,50</sup> makes a  $\pi$ -stack and a weak HB with H79<sup>2,45</sup> on TM2 in place of a HB with S<sup>2,45</sup> as in the  $\beta$ -adrenergic and adenosine A2A receptors (PDB ID 3EML)<sup>46</sup> and N<sup>2,45</sup> in the case of rhodopsin.

The most conserved class A GPCR residue on TM3, namely, R134<sup>3,50</sup> in CXCR4, has no partner acidic residue on TM6 unlike the other class A GPCRs with crystal structures. Thus the “ionic lock” is absent in CXCR4 receptor, since there is no acidic residue in the vicinity of this R134<sup>3,50</sup> residue, even in the intracellular loops 2 and 3. Our structural model shows three possible conformations for TM3, that places R134<sup>3,50</sup> slightly differently in the three conformations as shown in Figure 2A. In one of these conformations R134<sup>3,50</sup> makes a cation  $\pi$ -interaction with Y302<sup>7,53</sup> as shown in Figure 2B and in another conformation, D133<sup>3,49</sup> makes a two way HB with R134<sup>3,50</sup> and R146 on ICL2.

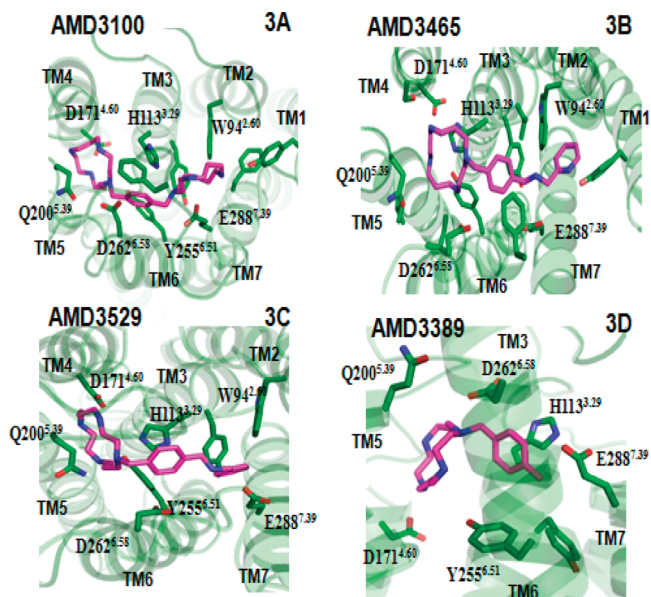


**Figure 3.** Best docked conformations of the mono- and bicyclam compounds after LITiCon procedure of receptor optimization for each ligand. Ligands are shown in magenta with their nitrogen atoms in blue. Residues making interactions with the ligands are in green stick.

**Predicted Binding Sites of Cyclam Compounds in CXCR4.** *Predicted Binding Site of Bicyclam Compound AMD3100 and its Cu<sup>2+</sup> Derivative.* The predicted binding site of AMD3100 is located between all the seven TM helices with the residues making strong interactions shown in Figure 3A. Acidic residues E288<sup>7,39</sup>, D262<sup>6,58</sup>, and D171<sup>4,60</sup> show favorable electrostatic interactions with the nitrogens on the cyclam rings. The acidic residues D181 and D182 in extracellular loop 2 (ECL2), D275 and E277 on ECL3 also contribute to ligand binding (omitted in the figure for clarity). Q200<sup>5,39</sup> makes a HB with the cyclam nitrogen. Aromatic residues such as Y45<sup>1,39</sup>, W94<sup>2,60</sup>, H113<sup>3,29</sup>, Y116<sup>3,32</sup>, Y255<sup>6,51</sup>, F292<sup>7,43</sup> and F276 (ECL3) also show strong van der Waals interactions with the ligand. The residues H113<sup>3,29</sup>, Y116<sup>3,32</sup>, Y255<sup>6,51</sup> make aromatic π-stacking contacts with the phenyl ring in the linker between the two cyclam rings. Residues I259<sup>6,55</sup> and I204<sup>5,43</sup> contribute to the hydrophobic interaction with the ligand. Site directed mutagenesis results show that the residue mutation to alanine of the following residues have the strongest effect on AMD3100 binding: E288<sup>7,39</sup>, D262<sup>6,58</sup>, D171<sup>4,60</sup>, Y45<sup>1,39</sup>, W94<sup>2,60</sup>, and Y116<sup>3,32</sup>.<sup>20–22</sup> Our results are in good agreement with these mutation results and further predict other residues that can affect AMD3100 binding. It is important to note that some of the residues like Y45<sup>1,39</sup>, W94<sup>2,60</sup> showed substantial conformational rearrangement upon AMD3100 binding, and this effect was captured by the LITiCon procedure. This conformational change leads to a selective “conformational mode” in the receptor that satisfies all the mutational data, and this cannot be achieved by receptor fixed docking methods. Several other interhelical contact rearrangements resulting from the helical movement during LITiCon include the formation of a tight interhelical HB between N56<sup>1,50</sup> and D84<sup>2,50</sup>, R134<sup>3,50</sup> and Y302<sup>7,53</sup> (2.91 Å), and between R134<sup>3,50</sup> and T240<sup>6,36</sup>.

*Binding Site of Cu<sup>2+</sup>-Bound AMD3100.* When Cu<sup>2+</sup> binds to the cyclam ring, the lone pair on the nitrogen atoms of the cyclam interact with the metal center, leading to a smaller

volume of the cyclam ring. Thus there is a conformational change in the mono- and bicyclam ligand when bound to Cu<sup>2+</sup>, leading to a shrinkage in the volume of the cyclam ring. Residues D262<sup>6,58</sup>, and E288<sup>7,39</sup>, each coordinate with the Cu<sup>2+</sup> in each cyclam ring, and aromatic residues Y45<sup>1,39</sup>, W94<sup>2,60</sup>, H113<sup>3,29</sup>, Y116<sup>3,32</sup>, and Y255<sup>6,51</sup> show favorable van der Waals interactions with the ligand. Much weaker contacts are observed with residues L108<sup>3,24</sup>, K110<sup>3,26</sup>, V112<sup>3,28</sup>, T117<sup>3,33</sup>. One major difference in the binding site is that the interaction energy of D171<sup>4,60</sup> with the ligand is much weaker in the Cu<sup>2+</sup> loaded AMD3100, than in AMD3100. Additional residues A175, S178, E179, A180 and D181 from ECL2 and L266, E275, E277 from ECL3 loops exhibit weak interaction with the ligand. However, F276 shows a favorable π-stack interaction with the phenyl ring between the two cyclam rings in AMD3100. It should be noted that residues Y45<sup>1,39</sup>, and W94<sup>2,60</sup> are brought in the vicinity of the binding pocket by helical rotational optimization in LITiCon. The interhelical HB between N56<sup>1,50</sup> and D84<sup>2,50</sup> is strengthened upon ligand binding compared to the structural model with no ligand bound. The ionic lock is absent in CXCR4 and instead the cation pi interaction between R134<sup>3,50</sup> and Y302<sup>7,53</sup> is strengthened in the AMD3100 bound structure.

*Predicted Binding Site of AMD3465 with and without Cu<sup>2+</sup>.* AMD3465 inhibitor is a monocyclam derivative of the bicyclam AMD3100 ligand, with a pyridine ring replacing one of the cyclam rings in AMD3100. In the predicted binding site of AMD3465 with and without Cu<sup>2+</sup>, the cyclam ring is located between helices TM3, TM4, TM5 and TM6 helices, the phenyl ring in the linker region interacts with the aromatics residues in TM3 and TM6, and the pyridine is located in the region between TM1, TM2 and TM7 (see Figure 3B). Residue D262<sup>6,58</sup> makes the strongest electrostatic contribution to the cyclam ring with this contribution increasing when the Cu<sup>2+</sup> is bound. The nitrogen on the cyclam ring coordinates weakly with D171<sup>4,60</sup>, while E288<sup>7,39</sup> makes a HB with the secondary amine group in the alkyl linker region and the nitrogen on the pyridine ring. There is a tight π-stacking interaction between H113<sup>3,29</sup>, Y116<sup>3,32</sup> on TM3, the aromatic phenyl ring in the linker region of the ligand, and F276 on ECL3. W94<sup>2,60</sup> and Y45<sup>1,39</sup> make aromatic π-stacking contact with the pyridine ring. These results are in agreement with the site directed mutagenesis data.<sup>20–22</sup> Residues A175, A180, and D181 on ECL2 show van der Waals interaction with the ligand. Residues in the TM region showing weak interaction with the ligand are K38<sup>1,32</sup>, L41<sup>1,35</sup>, P40<sup>1,34</sup>, and Y45<sup>1,39</sup> on TM1, A95<sup>2,61</sup>, and V96<sup>2,62</sup> on TM2, V112<sup>3,28</sup> on TM3, G197<sup>5,36</sup>, F199<sup>5,38</sup>, Q200<sup>5,39</sup>, F201<sup>5,40</sup>, H203<sup>5,42</sup>, and I204<sup>5,43</sup>, on TM5, Y255<sup>6,51</sup>, and I259<sup>6,57</sup> on TM6 and F292<sup>7,43</sup> on TM7. Wong et al.<sup>22</sup> showed through mutagenesis that H281<sup>7,32</sup> is a selective residue for AMD3465, and we find that this residue enters the predicted binding site during the receptor flexible docking using LITiCon. The residues in the binding site are essentially the same with and without Cu<sup>2+</sup> bound AMD3465. The Cu<sup>2+</sup> binding to AMD3465 shrinks the cyclam ring. The interhelical HB between N56<sup>1,50</sup> and D84<sup>2,50</sup> are tightened upon AMD3465 binding. We observe a HB between R134<sup>3,50</sup> and T240<sup>6,36</sup> and also between R134<sup>3,50</sup> and Y302<sup>7,53</sup>.

*Predicted Binding Site of AMD3529 with and without Cu<sup>2+</sup>.* AMD3529 is another monocyclam derivative inhibitor similar to AMD3465 with the pyridine ring being replaced

by a phenyl ring. The binding site location of AMD3529 with and without Cu<sup>2+</sup> are similar, and located between TM2 through TM7. The residues in the binding pocket of AMD3529 are shown in Figure 3C. The interaction of the phenyl ring is more biased toward the aromatic residues W94<sup>2.60</sup> and H113<sup>3.29</sup> on TM2 and TM3, respectively, and does not involve Y45<sup>1.39</sup> on TM1. On the other hand AMD3465 makes good contact with Y45<sup>1.39</sup>, and this is consistent with the site directed mutagenesis data for AMD3465.<sup>22</sup> Another feature that distinguishes the binding site of AMD3529 from that of AMD3465 is the interaction with H281<sup>7.32</sup>. This residue does not make any substantial contact with AMD3529. H113<sup>3.29</sup> makes a strong contact with the central phenyl ring in AMD3529, also in agreement with the site directed mutagenesis data 22. E288<sup>7.39</sup> makes a HB with the alkyl amine group in the linker region while D262<sup>6.58</sup> does not make contact with the ligand, unlike AMD3465. A weak HB is formed between D171<sup>4.60</sup> and one of the nitrogens in the cyclam ring. Q200<sup>5.39</sup> makes a strong HB with another nitrogen of the cyclam ring. Y255<sup>6.51</sup> and F276 on ECL3 make strong aromatic contact with the central phenyl ring in the linker region. The Cu<sup>2+</sup> binding to AMD3529 shrinks the cyclam ring as in AMD3465. The cyclam ring is located in the region between TM4 and TM5. D171<sup>4.60</sup> exhibits a contact with the monocyclam, followed by the  $\pi$ -stacking between the phenyl ring and H113<sup>3.29</sup> on TM3 and the aromatic phenyl ring of F276 on ECL3. A175 shows a favorable van der Waals interaction with the ring. Q200<sup>5.39</sup> as well as Y255<sup>6.51</sup> make HBs with the nitrogens of the cyclam ring. W94<sup>2.60</sup> and Y45<sup>1.39</sup> in this complex conformation is out of interaction range with the ligand in this pose. D262<sup>6.58</sup> makes a strong HB with the alkyl amine group as in the linker region of the original compound, while E288<sup>7.39</sup> loses its contact because of the shrinkage of the cyclam ring. Also, this conformation shows that the contact between residues N56<sup>1.50</sup> and D84<sup>2.50</sup> is broken upon AMD3529 with Cu<sup>2+</sup> binding. Interestingly, HB between R134<sup>3.50</sup> and T240<sup>6.36</sup> and R134<sup>3.50</sup> and Y302<sup>7.53</sup> observed in AMD3465 case are not present here.

*Predicted Binding Site of AMD3389 with and without Cu<sup>2+</sup>.* AMD3389 is also a monocyclam derivative with a methyl group replacing a longer phenylmethyl amine group in AMD3529. The predicted binding site of AMD3389 with and without Cu<sup>2+</sup>, has the cyclam ring located between helices TM3, TM4, and TM5. The phenyl ring in the linker region interacts with the aromatics residues in TM3 and TM6 while the methyl group is located in the region between TM3, TM6, and TM7 (see Figure 3D). Residue D171<sup>4.60</sup> makes a HB with the cyclam nitrogen, while D262<sup>6.58</sup> shows weak interaction with the cyclam ring in agreement with mutagenesis data. There is aromatic  $\pi$ -stacking interaction of the phenyl ring in the ligand with H113<sup>3.29</sup> and Y116<sup>3.32</sup> on TM3, F276 on ECL3, and Y255<sup>6.51</sup> on TM6. W94<sup>2.60</sup> and Y45<sup>1.39</sup> make aromatic  $\pi$ -stacking contact with others residues but not with the ligand. Q200<sup>5.39</sup> interacts weakly with the cyclam ring. Residues A175<sup>4.64</sup>, E179, and A180 on ECL2 show van der Waals interaction with the ligand. Other residues in the TM region showing interaction with the ligand are V114<sup>3.30</sup> and T117<sup>3.33</sup> on TM3, H203<sup>5.42</sup> and G207<sup>5.46</sup> on TM5, I256<sup>6.52</sup> on TM6, and F292<sup>7.43</sup> on TM7. Rosenkilde et al.<sup>21</sup> through mutagenesis showed that the mutation of E288<sup>7.39</sup>A leads to 15-fold decrease in binding affinity of AMD3389, but we

find that this residue makes only a very weak interaction with the methyl group. When Cu<sup>2+</sup> is bound in the cyclam ring, we observed that the original compound and its copper derivative share the same the binding site. The Cu<sup>2+</sup> binding to AMD3389 shrinks the cyclam ring as in the other monocyclam compounds and the binding site of the phenyl ring in AMD3389 is now confined between TM3 and TM5. The interhelical HB between K146<sup>3.62</sup> and D74<sup>2.40</sup> is present in both AMD3389 and its copper derivative. We observe two HBs between R134<sup>3.50</sup> and T240<sup>6.36</sup> and between R134<sup>3.50</sup> and Y302<sup>7.53</sup> similar as in the other monocyclams.

*Receptor Flexible Modeling of Antagonist Binding Site and Agreement with Experiments.* This study addresses the challenge of determining a unique binding mode for cyclam antagonists of CXCR4, that explains the experimental mutagenesis results. Site directed mutagenesis studies have implicated residues on TM1, TM2, TM3, TM4, TM6, and TM7 in the binding of the AMD series of compounds.<sup>20–22,47–49</sup> A single ligand binding mode that elucidates all of these residue contacts on TM helices that are distant such as TM2 and TM5, is difficult to obtain using homology models of CXCR4 derived from other class A GPCR crystal structures. Therefore, existing modeling studies<sup>22</sup> that rely on a fixed receptor backbone conformation suggest the possibility of multiple binding modes for each of the mono and bicyclam compounds that collectively account for all the site directed mutagenesis results. In the present study, we have used the computational method LITiCon to refine the ab initio CXCR4 model bound to several mono and bicyclam antagonists. Contrary to the previous report,<sup>22</sup> we were able to obtain a single binding mode for each of the antagonists that explain the mutagenesis data. This improved agreement with experiments is attributed to our binding site refinement protocol, which takes into account the receptor backbone changes selective and unique to each ligand. Figure 4 shows the binding site of the AMD compounds in the original CXCR4 model predicted using MembStruk, and the ligand optimized structures refined using LITiCon. We have calculated the interaction energy between the ligands and the residues in the binding site (residues within 5 Å of the ligand). Several of the experimentally implicated residues were already present inside the binding pocket in the original MembStruk CXCR4 model. These are Y45<sup>1.39</sup>, H113<sup>3.29</sup>, A175<sup>4.64</sup>, Q200<sup>5.39</sup>, I259<sup>6.55</sup>, D262<sup>6.58</sup>, and E288<sup>7.39</sup>. Receptor backbone optimization using LITiCon leads to small changes in TM1, TM3, TM4 and TM6 which improves the contacts with these residues as shown in Figure 4. Several other residue contacts were completely outside the binding pocket in the original CXCR4 model: W94<sup>2.60</sup> on TM2 and H281<sup>7.32</sup> on TM7. Mutating W94<sup>2.60</sup> to Ala reduces AMD3100 binding by 14-fold and AMD3465 binding by 90-fold.<sup>22</sup> While H281A mutation does not affect binding of AMD3100, this mutation reduces binding of AMD3465 by 4600 fold.<sup>21,22</sup> In the AMD3100 bound structural model, LITiCon backbone optimization brings only W94<sup>2.60</sup> inside the binding pocket, while with the AMD3465 bound structure both W94<sup>2.60</sup> and H281<sup>7.32</sup> come in contact with the ligand (Figure 4). In AMD3100 stabilized structure, H281<sup>7.32</sup> does not contact the ligand, which is in agreement with experiments (Figure 5). Thus the AMD3100 and AMD3465 optimized receptor structures differ mainly in the orientation of TM7. Since both these compounds act as

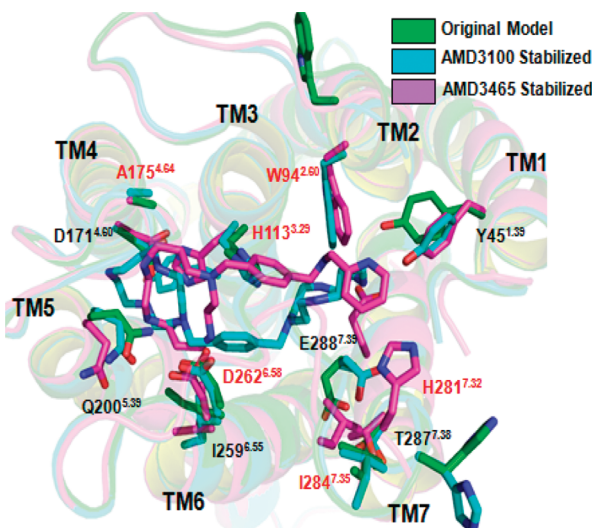


**Figure 4.** Comparison of receptor conformations for AMD3100 (in turquoise) and AMD3465 (in cyan) after LITiCon rotations in the transmembrane helices with the original receptor conformation (in green). Residues labeled in red show strong interaction with the ligand. Predicted docked pose of AMD3465. The central aromatic ring of the ligand is interacting with H113<sup>3,29</sup>. In the AMD3100 binding pocket, the central aromatic ring is located closer to TM6 and further away from H113<sup>3,29</sup>. This explains the reduced binding affinity of AMD3465 toward the H113A mutant compared to AMD3100.

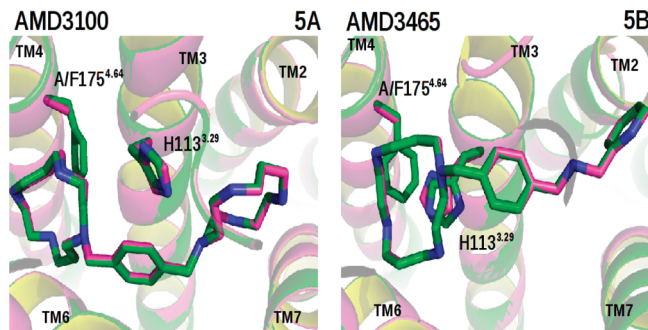


**Figure 5.** Mutation A175<sup>4,64</sup> to Phe in our CXCR4 model in docked poses of AMD3100 and AMD3465 compounds. Our predictions indicate that the cyclam ring of AMD3465 is closer to A175<sup>4,64</sup> compared to AMD3100 as shown in **5A** and **5B**. This mutation introduces a steric clash with the cyclam ring of AMD3465 reducing the binding affinity and stability. In the AMD3100 binding pocket, mutating A175<sup>4,64</sup> to Phe does not affect the rotamer preference of H113<sup>3,29</sup>.

inhibitors to CXCL12 binding, this indicates the possibility of existence of two alternative inactive states. This hypothesis draws support from the experimental data. While the binding affinities of AMD3100 and AMD3465 are similar (measured using competition binding with <sup>125</sup>I antibody 12G5), 0.89 and 0.11  $\mu$ M, AMD3465 is 3-fold more effective in inhibiting CXCL12 mediated activation compared to AMD3100.<sup>21</sup> Thus it is possible that AMD3465 stabilizes a receptor state, which shows lower affinity toward the G-protein Gq14myr compared to the AMD3100 stabilized state. Thus our findings are in agreement with the experimental mutagenesis data.

**Differences between Bicyclam (AMD3100) and Monocyclam (AMD3465) Binding Sites.** Both AMD3100 and AMD3465 are chemically similar, but structurally distinct compounds. Due to the substitution of one cyclam ring by an aryl ring, AMD3465 is smaller in size compared to AMD3100. Thus the binding pocket of AMD3465 is likely

to be more compact compared to that of AMD3100. In the previous section, we have shown that the binding pockets of both the compounds differ from one another in the backbone orientation of TM7. In the AMD3465 binding pocket, the side chain of H281<sup>7,32</sup> extends into the binding pocket contacting the aryl moiety of the ligand (Figure 4). In the AMD3100 binding pocket, H281<sup>7,32</sup> faces away from the binding pocket opening up the protein cavity, thus facilitating binding of the bulky cyclam ring. In our predicted AMD3465-optimized CXCR4 model, the polar nitrogen of H281<sup>7,32</sup> is well positioned to form HB with the nitrogen atom on the aryl ring. This observation is in agreement with the mutagenesis results. For compounds such as AMD3529, where the nitrogen on the aryl ring is replaced by carbon, the H281A mutant does not show any decrease in binding affinity compared to wild type.<sup>21</sup> Thus our computational model in conjunction with the mutagenesis data suggests a HB contact between H281<sup>7,32</sup> and the aryl moiety of AMD3465.

In our predicted AMD3465 binding pocket, the central aromatic ring of the ligand is close to TM3 and thus tightly packed against H113<sup>3,29</sup> (Figure 4). In contrast, in the AMD3100 binding pocket, the central aromatic ring is located closer to TM6 and further away from H113<sup>3,29</sup>. This explains the reduced binding affinity of AMD3465 toward the H113A mutant compared to AMD3100 (28-fold reduction for AMD3465 vs 2-fold for AMD3100). Besides TM3, the A175F mutation on TM4 also shows a larger effect on AMD3465 binding compared to AMD3100. To this end, we mutated A175<sup>4,64</sup> to Phe in our CXCR4 model and analyzed the binding of the AMD compounds in the mutant model. According to our predictions, the cyclam ring of AMD3465 is closer to A175<sup>4,64</sup> compared to AMD3100 (see Figure 5A and B). Thus replacing A175<sup>4,64</sup> with the bulky side chain of Phe introduces a steric clash with the cyclam ring of AMD3465 reducing the binding affinity. Besides this, our model also predicts the involvement of H113<sup>3,29</sup> in enhancing the effect of the A175F mutant toward AMD3465. Since A175<sup>4,64</sup> is facing TM3, mutating it to Phe brings the side chain of A175F<sup>4,64</sup> in close contact with H113<sup>3,29</sup>. To understand the effect of A175F<sup>4,64</sup> on the rotamer preference of H113<sup>3,29</sup>, we optimized the side chain of H113<sup>3,29</sup> in presence of A175F<sup>4,64</sup> using the side chain reassignment program SCREAM<sup>50</sup> and found that H113<sup>3,29</sup> assumes a different side chain rotamer in the presence of A175F<sup>4,64</sup> compared to A175<sup>4,64</sup> (Figure 5B). Thus the contact between H113<sup>3,29</sup> and AMD3465 is destabilized in the A175F mutant. In the AMD3100 binding pocket, because of the additional space between TM3 and the aromatic linker of the ligand, H113<sup>3,29</sup> faces away from A175<sup>4,64</sup> (Figure 5A). Hence mutating A175<sup>4,64</sup> to Phe does not affect the rotamer preference of H113<sup>3,29</sup> in the AMD3100 bound model.

**Analogy of CXCR4 Allosteric Pharmacophore with other Chemokine Receptors.** Besides those of CXCR4, allosteric antagonists that bind to the transmembrane domains of other chemokine receptors have been identified, such as RS-102895 for CCR2,<sup>51</sup> UCB35625 and CH0076789 for CCR3,<sup>52</sup> Aplaviroc, SCH-C, TAK-779 for CCR5,<sup>53</sup> and Repertaxin for CXCR1/CXCR2.<sup>54</sup> These compounds do not show any chemical structural similarities or share any common template functional groups. However, we observe that the residues that these antagonists contact are either conserved

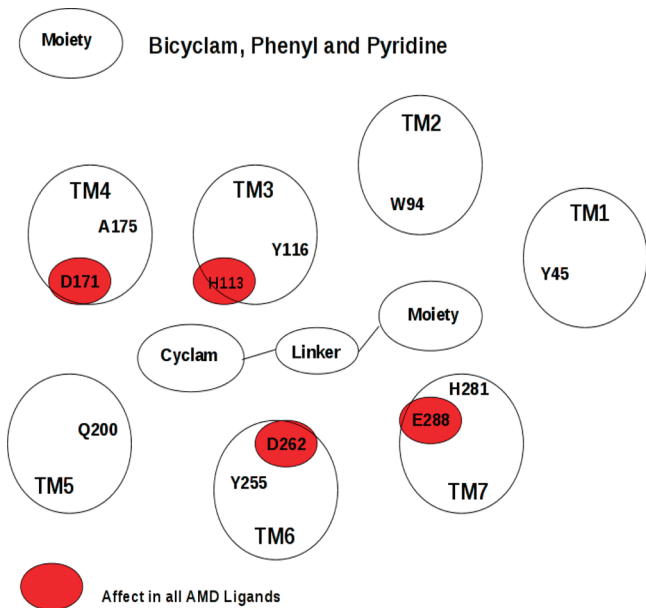


**Figure 6.** Pharmacophore that describes those residues involved in the binding of allosteric antagonists in chemokine receptors. Several key residues involved in the functioning of the AMD compounds are shown in red also important for the activity of small molecule ligands for other chemokine receptors.

in many chemokine receptors or their positions are always involved in antagonist binding even when not conserved. Comparing the binding pockets of multiple chemokine receptors, we can identify the conserved residues that are involved in the binding of several antagonists. These residues are Y<sup>1,39</sup>, W<sup>2,60</sup>, H(Y)<sup>2,29</sup>, Y<sup>3,32</sup>, I<sup>6,55</sup>, and E<sup>7,39</sup>. For example, Y45<sup>1,39</sup> on TM1 in CXCR4 is implicated in the binding of mono and bicyclam compounds.<sup>22</sup> This residue is conserved in all chemokine receptors and is experimentally implicated in the functioning of multiple allosteric antagonists. In CCR3, the homologous residue Y41<sup>1,39</sup> when mutated to Ala abolishes binding of both UCB35625 and CH0076789.<sup>52</sup> In CCR5, this residue is Y37<sup>1,39</sup> and alanine mutation abolishes binding of SCH-C and reduces TAK-779 binding by 98-fold.<sup>53</sup> In CXCR1, the homologous mutation Y46A<sup>1,39</sup> abolishes Repertaxin mediated inhibitory effect on cell migration.<sup>54</sup> Some of the positions in the TM regions are involved in binding even if the residues at these positions are not strictly conserved. In CXCR4, D171<sup>4,60</sup> on TM4 is implicated in the binding of mono and bicyclam compounds. Mutating D171<sup>4,60</sup> to N reduces binding of AMD3100 and AMD3465 by 11- and 27-fold, respectively.<sup>22</sup> This residue is not conserved among the chemokine receptors. However the homologous residue G163<sup>4,60</sup> in CCR5 when mutated to Arg abolishes the binding of Aplaviroc, but only marginally affects the binding of SCH-C and TAK-779.<sup>53</sup> In Figure 6, we show the pharmacophore or the residues involved in the binding of allosteric antagonists in chemokine receptors. Many of the key residues involved in the functioning of the AMD compounds are also important for the activity of small molecule ligands for other chemokine receptors. This knowledge would be important for the future designing of drugs for targeting multiple chemokine receptors, as well as discovering subtype selective compounds for this family of chemokine receptors.

## CONCLUSIONS

We have presented a comprehensive description of the binding of cyclam-based antagonists to human CXCR4, explaining the experimental mutation data. Using the ab initio Membstruk structure prediction method, we have predicted an ensemble of structural models for CXCR4, without using any homology information from other GPCR crystal structures. We have further predicted the putative binding sites of mono and bicyclam antagonists. The predicted binding modes of the mono and bicyclam antagonists showed contacts with many of the residues that are implicated in antagonist binding through mutagenesis studies. However, to account for all the mutagenesis data with a single binding model, we used the LITiCon method that allows optimization of the orientation of the TM helices in response to ligand binding. Performing LITiCon on the AMD3100 bound CXCR4 structure brings W94<sup>2,63</sup> in contact with the ligand, while the same treatment on the AMD3465 bound receptor brings both W94<sup>2,63</sup> and H281<sup>7,32</sup> inside the binding cavity, in agreement with the mutation data. Therefore by including receptor backbone flexibility, it is possible to consolidate all the mutation data pertaining to the binding of the cyclam compounds. Our studies also suggest that the CXCR4 conformation stabilized by AMD3100 differs slightly from the one stabilized by AMD3465, mainly in the orientation of TM7. This may explain the improved efficacy of AMD3465 over AMD3100 in inhibiting the action of CXCL12.

There are several notable differences in the binding site of the mono and bicyclam antagonists. The smaller monocyclam compound, AMD3465 has the H281<sup>7,32</sup> in the binding cavity, making a HB with the nitrogen atom in the aryl ring, while in the larger AMD3100 bound conformation, H281<sup>7,32</sup> moves away from the binding site, opening up the binding pocket. This is in accordance to the mutation results, that H281<sup>7,32</sup> selectively interacts with AMD3465 and not with AMD3100. We have also explained the increased effect of H113A and decreased effect of A175F mutations on AMD3465 binding compared to AMD3100. Transition metal loading is important to using the cyclam compounds for positron emission tomography.<sup>55</sup> We have studied the effect of transition metals on the binding site of the cyclam compounds. The presence of transition metal ions in the cyclam compounds shrinks the size of the cyclam rings to which the receptor conformations respond. Residue D262<sup>6,58</sup> plays an important role in bonding to the copper ion in the monocyclam compounds while residue E288<sup>7,39</sup> seems to prevail in binding of the bicyclam compounds over the residue D262<sup>6,58</sup>. We have derived a pharmacophore for the cyclam compounds binding and compared it to the binding site of allosteric antagonists in other chemokine receptors. Many of the residues that contact allosteric antagonists in the chemokine receptors are conserved. Among the CXCR4 residues that contact the mono and bicyclam compounds, the residues Y<sup>1,39</sup>, W<sup>2,60</sup>, H(Y)<sup>2,29</sup>, Y<sup>3,32</sup>, I<sup>6,55</sup>, and E<sup>7,39</sup> are conserved among many chemokine receptors and are implicated in allosteric antagonist binding. This indicates that the binding site predicted for the mono and bicyclam compounds is a potential allosteric binding pocket binding pocket and this would be useful in designing dual antagonists for CXCR4 and other chemokine receptors.

## REFERENCES AND NOTES

- (1) Rot, A.; von Andrian, U. H. Chemokines in Innate and Adaptive Host Defense: Basic Chemokine Grammar for Immune Cells. *Annu. Rev. Immunol.* **2004**, *22*, 891–928.
- (2) Lefkowitz, R. Historical Review: A Brief History and Personal Retrospective of Seven-Transmembrane Receptors. *Trends Pharmacol. Sci.* **2004**, *25*, 413–422.
- (3) Schyler, S.; Horuk, R. I Want a New Drug: G-Protein-Coupled Receptors in Drug Development. *Drug Discovery Today.* **2006**, *11*, 481–493.
- (4) Horuk, R. Molecular Properties of the Chemokine Receptor Family. *Trends Pharmacol. Sci.* **1994**, *15*, 159–65.
- (5) Rossi, D.; Zlotnik, A. The Biology of Chemokines and their Receptors. *Annu. Rev. Immunol.* **2000**, *18*, 217–242.
- (6) Bacon, K.; Baggolini, M.; Horuk, R.; Lindley, I.; Mantovani, A.; Matsushima, K.; Murphy, P.; Nomiyama, H.; Oppenheim, J.; Rot, A.; Schall, T.; Tsang, M.; Thorpe, R.; Van Damme, J.; Wadhwa, M.; Yoshie, O.; Zlotnik, A.; Zoon, K. Chemokine/Chemokine Receptor Nomenclature IUIS/WHO Subcommittee on Chemokine Nomenclature. *J. Immunol. Meth.* **2002**, *262*, 1–3.
- (7) Dar, A.; Goichberg, P.; Shinder, V.; Kalinkovich, A.; Kollet, O.; Netzer, N.; Margalit, R.; Zsak, M.; Nagler, A.; Hardan, I.; Resnick, I.; Rot, A.; Lapidot, T. Chemokine Receptor CXCR4-dependent Internalization and Resecretion of Functional Chemokine SDF-1 by Bone Marrow Endothelial and Stromal Cells. *Nat. Immunol.* **2005**, *6*, 1038–1046.
- (8) Onuffer, J.; Horuk, R. Chemokines, Chemokine Receptors and Small-Molecule Antagonists: Recent Developments. *Trends Pharmacol. Sci.* **2002**, *23*, 459–467.
- (9) De Clercq, E.; Yamamoto, N.; Pauwels, R.; Baba, M.; Schols, D.; Nakashima, H.; Balzarini, J.; Debyser, Z.; Murrer, B. A.; Schwartz, D. Potent and Selective Inhibition of Human Immunodeficiency Virus (HIV)-1 and HIV-2 Replication by a Class of Bicyclams Interacting with a Viral Uncoating Event. *Proc. Natl. Acad. Sci. U.S.A.* **1992**, *89*, 5286–5290.
- (10) Hatse, S.; Princen, K.; Clercq, E.; Rosenkilde, M.; Schwartz, T.; Hernandezabed, P.; Skerlj, R.; Bridger, G.; Schols, D. AMD3465, A Monomacrocyclic CXCR4 Antagonist and Potent HIV Entry Inhibitor. *Biochem. Pharmacol.* **2005**, *70*, 752–761.
- (11) Fricker, S. P.; Anastassov, V.; Cox, J.; Darkes, M. C.; Grujic, O.; Idzan, S. R.; Labrecque, J.; Lau, G.; Mosi, R. M.; Nelson, K. L. Characterization of the Molecular Pharmacology of AMD3100: A Specific Antagonist of the G-Protein Coupled Chemokine Receptor, CXCR4. *Biochem. Pharmacol.* **2006**, *72*, 588–596.
- (12) Bodart, V.; Anastassov, V.; Darkes, M.; Idzan, S.; Labrecque, J.; Lau, G.; Mosi, R.; Neff, K.; Nelson, K.; Ruzek, M. Pharmacology of AMD3465: A Small Molecule Antagonist of the Chemokine Receptor CXCR4. *Biochem. Pharmacol.* **2009**, *78*, 993–1000.
- (13) Nagasawa, T.; Hirota, S.; Tachibana, K.; Takakura, N.; Nishikawa, S.; Kitamura, Y.; Yoshida, N.; Kikutani, H.; Kishimoto, T. Defects of B-cell Lymphopoiesis and Bone-Marrow Myelopoiesis in Mice Lacking the CXC chemokine PBSF/SDF-1. *Nature* **1996**, *382*, 635–638.
- (14) Aiuti, A.; Webb, I. J.; Bleul, C.; Springer, T.; Gutierrez-Ramos, J. C. The Chemokine SDF-1 Is a Chemoattractant for Human CD34+ Hematopoietic Progenitor Cells and Provides a New Mechanism to Explain the Mobilization of CD34+ Progenitors to Peripheral Blood. *J. Exp. Med.* **1997**, *185*, 111–120.
- (15) Baggolini, M. Chemokines and Leukocyte Traffic. *Nature* **1998**, *392*, 565–568.
- (16) Peled, A.; Petit, I.; Kollet, O.; Magid, M.; Ponomaryov, T.; Byk, T.; Nagler, A.; Ben-Hur, H.; Many, A.; Shultz, L.; Lider, O.; Alon, R.; Zipori, D.; Lapidot, T. Dependence of Human Stem Cell Engraftment and Repopulation of NOD/SCID Mice on CXCR4. *Science* **1999**, *283*, 845–848.
- (17) De Clercq, E. The AMD3100 Story: The Path to the Discovery of a Stem Cell Mobilizer (Mozobil). *Biochem. Pharm.* **2009**, *77*, 1655–1664.
- (18) Hatse, S.; Princen, K.; Vermeire, K.; Gerlach, L. O.; Rosenkilde, M.; Schwartz, T.; Bridger, G.; De Clercq, R. I. K.; Schols, D. Mutations at the CXCR4 Interaction Sites for AMD3100 Influence Anti-CXCR4 Antibody Binding and HIV-1 Entry. *FEBS Lett.* **2003**, *546*, 300–306.
- (19) Trent, J. O.; Wang, Z.-x.; Murray, J. L.; Shao, W.; Tamamura, H.; Fujii, N.; Peiper, S. C. Lipid Bilayer Simulations of CXCR4 with Inverse Agonists and Weak Partial Agonists. *J. Biol. Chem.* **2003**, *278*, 47136–47144.
- (20) Rosenkilde, M. M.; Gerlach, L. O.; Jakobsen, J. S.; Skerlj, R. T.; Bridger, G. J.; Schwartz, T. W. Molecular Mechanism of AMD3100 Antagonism in the CXCR4 Receptor. *J. Biol. Chem.* **2004**, *279*, 3033–3041.
- (21) Rosenkilde, M. M.; Gerlach, L. O.; Hatse, S.; Skerlj, R. T.; Schols, D.; Bridger, G. J.; Schwartz, T. W. Molecular Mechanism of Action of Monocyclam versus Bicyclam Non-Peptide Antagonists in the CXCR4 Chemokine Receptor. *J. Biol. Chem.* **2007**, *282* (37), 27354–27365.
- (22) Wong, R. S. Y.; Bodart, V.; Metz, M.; Labrecque, J.; Bridger, G.; Fricker, S. P. Comparison of the Potential Multiple Binding Modes of Bicyclam, Monocyclam, and Noncyclam Small-Molecule CXC Chemokine Receptor 4 Inhibitors. *Mol. Pharmacol.* **2008**, *74*, 1485–1495.
- (23) Gerlach, L.; Skerlj, R.; Bridger, G.; Schwartz, T. Molecular Interactions of Cyclam and Bicyclam Non-peptide Antagonists with the CXCR4 Chemokine Receptor. *J. Biol. Chem.* **2001**, *276*, 14153–14160.
- (24) Gerlach, L. O.; Jakobsen, J. S.; Jensen, K. P.; Rosenkilde, M. R.; Skerlj, R. T.; Ryde, U.; Bridger, G. J.; Schwartz, T. W. Metal Ion Enhanced Binding of AMD3100 to Asp262 in the CXCR4 Receptor. *Biochemistry* **2003**, *42*, 710–717.
- (25) Ballesteros, J. A.; Weinstein, H. Integrated Methods for the Construction of Three-Dimensional Models and Computational Probing of Structure-Function Relations in G-Protein-Coupled Receptors. *Methods Neurosci.* **1995**, *25*, 366–366.
- (26) Hatse, S.; Princen, K.; Gerlach, L.; Bridger, G.; Henson, G.; De Clercq, E.; Schwartz, T.; Schols, D. Mutation of Asp and Asp of the Chemokine Receptor CXCR4 Impairs its Coreceptor Function for Human Immunodeficiency Virus-1 Entry and Abrogates the Antagonistic Activity of AMD3100. *Mol. Pharm.* **2001**, *60*, 164–173.
- (27) Trabanino, R. J.; Hall, S. E.; Vaidehi, N.; Floriano, W. B.; Kam, V. W. T.; Goddard, W. A. First Principles Predictions of the Structure and Function of G-Protein-Coupled Receptors: Validation for Bovine Rhodopsin. *Biophys. J.* **2004**, *86*, 1904–1921.
- (28) Hall, S. E. Development of a Structure Prediction Method for G-Protein Coupled Receptors. PhD Thesis, Caltech, Pasadena, CA, 2005.
- (29) Cherezov, V.; Rosenbaum, D. M.; Hanson, M. A.; Rasmussen, S. G. F.; Thian, F. S.; Kobilka, T. S.; Choi, H.-J.; Kuhn, P.; Weis, W. I.; Kobilka, B. K.; Stevens, R. C. High-Resolution Crystal Structure of an Engineered Human  $\beta$ 2-Adrenergic G Protein-Coupled Receptor. *Science* **2007**, *318*, 1258–1265.
- (30) Schertler, G. F. X. Structure of Rhodopsin. *Eye* **1998**, *12*, 504–510.
- (31) Scheerer, P.; Park, J. H.; Hildebrand, P. W.; Kim, Y. J.; Krauss, N.; Choe, H.-W.; Hofmann, K. P.; Ernst, O. P. Crystal Structure of the Ligand-Free G-Protein-Coupled Receptor Opsin. *Nature* **2008**, *454*, 183–187.
- (32) Park, J. H.; Scheerer, P.; Hofmann, K. P.; Choe, H.-W.; Ernst, O. P. Crystal Structure of Opsin in its G-Protein-Interacting Conformation. *Nature* **2008**, *455*, 497–502.
- (33) Fiser, A.; Sali, A. Modeller: Generation and Refinement of Homology-Based Protein Structure Models. *Methods Enzymol.* **2008**, *374*, 461–91.
- (34) Jorgensen, W. L.; Maxwell, D. S.; Tirado Rives, J. Development and Testing of the OPLS All-Atom Force Field on Conformational Energistics and Properties of Organic Liquids. *J. Am. Chem. Soc.* **1996**, *118*, 11225–11236.
- (35) Ghosh, A.; Rapp, C. S.; Friesner, R. A. Generalized Born Model Based on a Surface Integral Formulation. *J. Phys. Chem. B.* **1998**, *102*, 10983–10990.
- (36) Bhattacharya, S.; Hall, S. E.; Li, H.; Vaidehi, N. Ligand-Stabilized Conformational States of Human  $\beta$ 2 Adrenergic Receptor: Insight into G-Protein-Coupled Receptor Activation. *Biophys. J.* **2008**, *94*, 2027–2042.
- (37) Bhattacharya, S.; Hall, S. E.; Vaidehi, N. Agonist-Induced Conformational Changes in Bovine Rhodopsin: Insight into Activation of G-Protein-Coupled Receptors. *J. Mol. Biol.* **2008**, *382*, 539–555.
- (38) Bhattacharya, S.; Vaidehi, N. Computational Mapping of the Conformational Transitions in Agonist Selective Pathways of a G-Protein Coupled Receptor. *J. Am. Chem. Soc.* **2010**, *132*, 5205–5214.
- (39) McDonald, I. K.; Thornton, J. M. Satisfying Hydrogen Bonding Potential in Proteins. *J. Mol. Biol.* **1994**, *238*, 777–793.
- (40) Warne, T.; Serrano-Vega, M. J.; Baker, J. G.; Moukhametzianov, R.; Edwards, P. C.; Henderson, R.; Leslie, A. G. W.; Tate, C. G.; Schertler, G. F. X. Structure of a  $\beta$ 1-Adrenergic G-Protein-Coupled Receptor. *Nature* **2008**, *454*, 486–491.
- (41) Rasmussen, S. G. F.; Choi, H.-J.; Rosenbaum, D. M.; Kobilka, T. S.; Thian, F. S.; Edwards, P. C.; Burghammer, M.; Ratnala, V. R. P.; Sanishvili, R.; Fischetti, R. F.; Schertler, G. F. X.; Weis, W. I.; Kobilka, B. K. Crystal Structure of the Human  $\beta$ 2 Adrenergic G-Protein-Coupled Receptor. *Nature* **2007**, *450*, 383–387.
- (42) Palczewski, K.; Kumada, T.; Hori, T.; Behnke, C. A.; Motoshima, H.; Fox, B. A.; Le Trong, I.; Teller, D. C.; Okada, T.; Stenkamp, R. E.; Yamamoto, M.; Miyano, M. Crystal Structure of Rhodopsin: a G-Protein-Coupled Receptor. *Science* **2000**, *289*, 739–745.
- (43) Vaidehi, N.; Schlyer, S.; Trabanino, R. J.; Floriano, W. B.; Abrol, R.; Sharma, S.; Kochanny, M.; Koovakat, S.; Dunning, L.; Liang, M.; Fox, J. M.; de Mendonca, F. L.; Pease, J. E.; Goddard, W. A.; Horuk, R. Predictions of CCR1 Chemokine Receptor Structure and BX471 Antagonist Binding followed by Experimental Validation. *J. Biol. Chem.* **2006**, *281*, 27613–27620.

- (44) Hall, S. E.; Roberts, K.; Vaidehi, N. Position of Helical Kinks in Membrane Protein Crystal Structures and the Accuracy of Computational Prediction. *J. Mol. Graphics & Modell.* **2009**, *27*, 944–950.
- (45) Deupi, X.; Olivella, M.; Govaerts, C.; Ballesteros, J. A.; Campillo, M.; Pardo, L. Ser and Thr Residues Modulate the Conformation of Pro-Kinked Transmembrane Alpha-Helices. *Biophys. J.* **2004**, *86*, 105–115.
- (46) Jaakola, V.-P.; Griffith, M. T.; Hanson, M. A.; Cherezov, V.; Chien, E. Y. T.; Lane, J. R.; Ijzerman, A. P.; Stevens, R. C. The 2.6 Angstrom Crystal Structure of a Human A<sub>2A</sub> Adenosine Receptor Bound to an Antagonist. *Science* **2008**, *322*, 1211–1217.
- (47) Tian, S.; Choi, W.; Liu, D.; Pesavento, J.; Wang, Y.; An, J.; Sodroski, J.; Huang, Z. Distinct Functional Sites for Human Immunodeficiency Virus Type 1 and Stromal Cell-Derived Factor 1 Alpha on CXCR4 Transmembrane Helical Domains. *J. Virol.* **2005**, *79*, 12667–12673.
- (48) Choi, W.; Tian, S.; Dong, C.; Kumar, S.; Liu, D.; Madani, N.; An, J.; Sodroski, J.; Huang, Z. Unique Ligand Binding Sites on CXCR4 Probed by a Chemical Biology Approach: Implications for the Design of Selective Human Immunodeficiency Virus Type 1 Inhibitors. *J. Virol.* **2005**, *79*, 15398–15404.
- (49) Liang, X.; Parkinson, J. A.; Weishaupl, M.; Gould, R. O.; Paisey, S. J.; Park, H.; Hunter, T. M.; Blindauer, C. A.; Parson, S.; Sadler, P. J. Structure and Dynamics of Metallamacrocycles: Recognition of Zinc Xylyl-Bicyclam by an HIV coreceptor. *J. Am. Chem. Soc.* **2001**, *124*, 9105–9112.
- (50) Kam, V. W. T.; Goddard III, W. A. Flat-Bottom Strategy for Improved Accuracy in Protein Side-Chain Placements. *J. Chem. Theory Comput.* **2008**, *4*, 2160–2169.
- (51) Mirzaegaran, T.; Diehl, F.; Ebi, B.; Bhakta, S.; Polksy, I.; McCarley, D.; Mulkins, M.; Weatherhead, G. S.; Lapierre, J. M.; Dankwardt, J.; Morgans, D.; Wilhelm, R.; Jarnagin, K. Identification of the Binding Site for a Novel Class of CCR2b Chemokine Receptor Antagonists—Binding to a Common Chemokine Receptor Motif within the Helical Bundle. *J. Biol. Chem.* **2000**, *275*, 25562–25571.
- (52) Wise, E. L.; Duchesnes, C.; da Fonseca, P. C. A.; Allen, R. A.; Williams, T. J.; Pease, J. E. Small Molecule Receptor Agonists and Antagonists of CCR3 provide Insight into Mechanisms of Chemokine Receptor Activation. *J. Biol. Chem.* **2007**, *282*, 27935–27943.
- (53) Maeda, K.; Das, D.; Ogata-Aoki, H.; Nakata, H.; Miyakawa, T.; Tojo, Y.; Norman, R.; Takaoka, Y.; Ding, J. P.; Arnold, G. F.; Arnold, E.; Mitsuya, H. Structural and Molecular Interactions of CCR5 Inhibitors with CCR5. *J. Biol. Chem.* **2006**, *281*, 12688–12698.
- (54) Bertini, R.; Allegretti, M.; Bizzarri, C.; Moriconi, A.; Locati, M.; Zampella, G.; Cervellera, M. N.; Di Cioccio, V.; Cesta, M. C.; Galliera, E.; Martinez, F. O.; Di Bitondo, R.; Troiani, G.; Sabbatini, V.; D'Anniballe, G.; Anacardio, R.; Cutrin, J. C.; Cavalieri, B.; Mainiero, F.; Strippoli, R.; Villa, P.; Di Girolamo, M.; Martin, F.; Gentile, M.; Santoni, A.; Corda, D.; Poli, G.; Mantovani, A.; Ghezzi, P.; Colotta, F. Noncompetitive Allosteric Inhibitors of the Inflammatory Chemokine Receptors CXCR1 and CXCR2: Prevention of Reperfusion Injury. *Proc. Natl. Acad. Sci. U.S.A.* **2004**, *101*, 11791–11796.
- (55) Nimmagadda, S.; Pullambhatala, M.; Stone, K.; Green, G.; Bhujwalla, A. M. PomperMolecular Imaging of CXCR4 Receptor Expression in Human Cancer Xenografts with [<sup>64</sup>Cu]AMD3100 Positron Emission Tomography. *Cancer Res.* **2010**, *70*, 3935–44.

CI1003027